COMMISSION INTERNATIONALE
DES GRANDS BARRAGES

VINGT-CINQUIÈME CONGRÈS
DES GRANDS BARRAGES
Stavanger, Juin 2015

EVALUATION OF SEISMIC PERFORMANCE OF THE INTERFACE OF A COMPOSITE DAM AGAINST LARGE SCALE EARTHQUAKE MOTION [(*)]

Akira NAKAMURA
Councilor, the Japan Dam Engineering Center

Nario YASUDA
Senior Researcher, the Japan Dam Engineering Center

Takahiro KINOSHITA
Director, Chubetsu Dam Management Branch Office, Asahikawa River Office, Hokkaido Regional Development Bureau, Ministry of Land, Infrastructure, Transport and Tourism

Hitoshi ETOH
Chief Engineer, Project Management Office, Nippon Koei Co., Ltd.,

JAPAN

1. INTRODUCTION

This paper sets large-scale earthquake motion (Level 2 earthquake motion) for the part of a large-scale composite dam near the interface of its embankment dam (dam height: 78.5 m) and concrete dam (dam height: 86 m) in order to evaluate seismic performance, mainly near the interface. The structural design of the interface of Chubetsu Dam features connections in the plane direction with the concrete dam part within the range of the width of the core and filter, while in the shell part, the concrete dam part is enfolded. In the part near the interface, the embankment dam and concrete dam, which have different response characteristics, are connected, so a

---

[(*)] *Évaluation des performances sismiques de l'interface d'un barrage composite en cas de tremblement de terre de grande ampleur*

three-dimensional detailed model was prepared and FEM dynamic analysis of the composite dam under Level 2 earthquake motion was carried out to evaluate its seismic performance.

2. STRUCTURE AND EXECUTION METHOD OF THE INTERFACE

Fig. 1 and Fig. 2 are the longitudinal and lateral profiles respectively of the interface. The concrete dam part is enfolded into the embankment dam part. The height of the interface is 76 m and its gradient is 1:0.7.

The material zoning of the interface is, as shown in Fig. 3, contact clay, core with intermediate grain size (hereafter, intermediate core), and core, in that order, and thus the properties of the materials are gradually varied. The contact clay is highly plastic with a maximum particle diameter of 20 mm, and has a larger fine-grained fraction and higher water content than that in the core. Its layer thickness is a total of 20 cm consisting of one layer of 5 cm, and two layers of 7.5 cm, and it was compacted using a 16.7-kg air tamper and 53-kg tamper. The intermediate core material has a maximum grain size of 80 mm and its coarse large-grained constituent was removed to stand between the contact clay and the core in grain size distribution.

The intermediate core is 2 m wide horizontally and 10 cm thick, and was compacted with a 0.8-ton compact vibrating roller. The core material has the maximum grain size of 150 mm with the layer of 30 cm thick, and was compacted with an 11-ton vibrating roller.

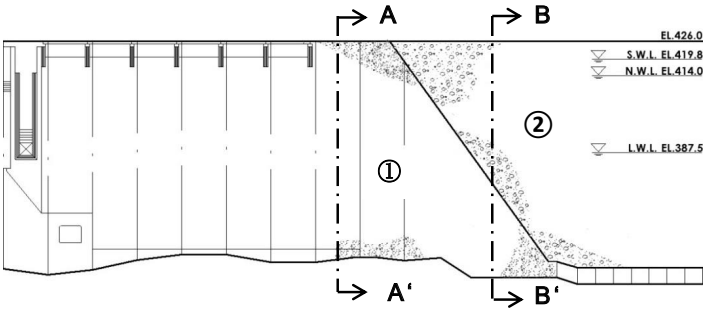

Fig. 1
Longitudinal profile of interface
Profil longitudinal de l'interface

1 Concrete dam — *1 Barrage en béton*
2 Embankment dam — *2 Barrage en remblai*

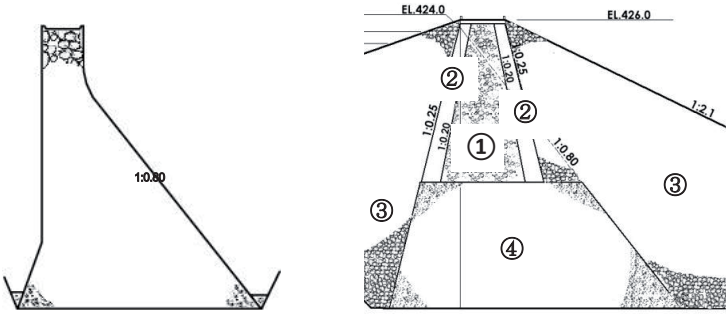

(1) **A-A'** section (2) **B-B'** section

Fig. 2
Lateral profile of interface
Profil latéral de l'interface

1 Core	*1 Noyau*
2 Filter	*2 Filtre*
3 Shell	*3 Recharge*
4 Concrete dam	*4 Barrage en béton*

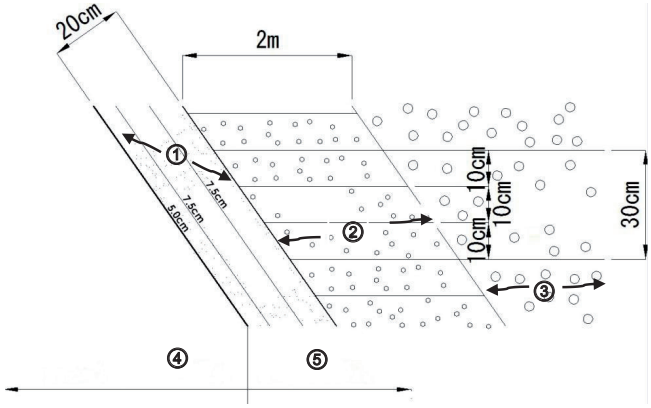

Fig. 3
Embankment material zoning of interface
Zonage de l'interface du remblai

1 Contact clay	*1 Argile de contact*
2 Intermediate core	*2 Noyau intermédiaire*
3 Main core	*3 Noyau principal*
4 Concrete dam	*4 Barrage en béton*
5 Embankment dam	*5 Barrage en remblai*

3. SETTING THE LARGE-SCALE EARTHQUAKE MOTION (LEVEL 2 EARTHQUAKE MOTION)

3.1. SELECTING THE HYPOTHETICAL EARTHQUAKES

According to the circular guidance (River Bureau, MLIT, 2005 [1]), Level 2 earthquake motion is estimated as the maximum influence at the dam site from now into the future.

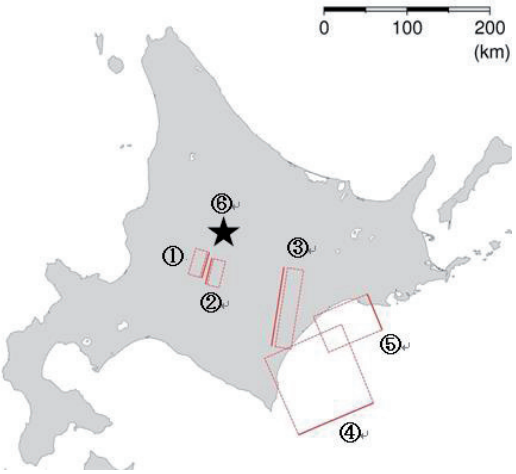

Fig. 4
Locations of Chubetsu Dam and hypothetical earthquake candidate (1) to (5) hypocenter faults
Emplacement du barrage de Chubetsu et des différentes failles pouvant constituer l'hypocentre (foyer) d'éventuels séismes (1) à (5)

1 West part of the Furano Fault Zone	*1 Partie ouest de la zone de la faille de Furano*
2 East part of the Furano Fault Zone	*2 Partie est de la zone de la faille de Furano*
3 Main part of the Tokachi Plain Fault Zone	*3 Partie principale de la zone de la faille de la plaine de Tokachi*
4 Tokachi Offshore Earthquake	*4 Séisme en mer au large de Tokachi*
5 Kushiro Offshore Earthquake	*5 Séisme en mer au large de Kushiro*
6 Location of Chubetsu Dam	*6 Emplacement du barrage de Chubetsu*

Using existing documentary sources, we investigated earthquakes which occurred near the object dam in the past, as well as active faults and plate boundary earthquakes which would severely impact the Chubetsu Dam, in order to select the

maximum assumption earthquake (MAE). We used the “specific attenuation formula for dams” to calculate the maximum acceleration at the dam site, and selected MAE candidates causing 100 cm/s^2 or higher acceleration. As a result, the following three fault zones were selected.

(1) West part of the Furano Fault Zone (magnitude: M7.2)
(2) East part of the Furano Fault Zone (magnitude: M7.2)
(3) Main part of the Tokachi Plain Fault Zone (magnitude: M8.0)

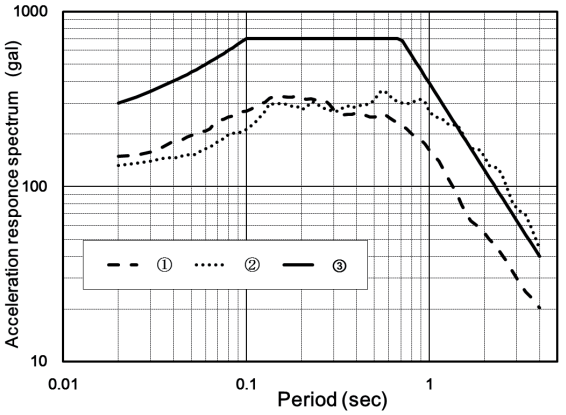

Fig. 5
Comparison of acceleration response spectra obtained according to the dam attenuation formula
Comparaison des spectres de réponse à l’accélération conformément à la formule d’atténuation du barrage

1 West part of the Furano Fault Zone	*1 Partie ouest de la zone de la faille de Furano*
2 Tokachi Offshore Earthquake	*2 Séisme en mer au large de Tokachi*
3 Lower limit acceleration response spectrum for earthquake resistance verification	*3 Spectre de la limite inférieure de la réponse à l’accélération en vue de vérifier la résistance aux séismes*

We similarly calculated the maximum acceleration at the dam site during a large offshore interplate earthquake, selecting two MAE candidates of 100 cm/s^2 or higher acceleration. Fig. 4 shows the locations of the hypocentral faults of the MAE candidate (1) to (5).

(4) Tokachi Offshore Earthquake (magnitude: M8.1)
(5) Kushiro Offshore Earthquake (magnitude: M7.5)

The “specific attenuation formula for dams “ is an earthquake motion prediction formula obtained by applying statistical regression method based on many earthquake records observed at dam sites in Japan, and it is one empirical method for predicting earthquake motion. Using this formula, it is possible to obtain the acceleration response spectrum at the dam location during a target earthquake by providing five fault parameters: the type of earthquake (earthquake caused by an inland active fault, inter plate (boundary) earthquake, or intraplate earthquake, etc.), earthquake magnitude, shortest distance or equivalent hypocentral distance from the dam to the hypocentral fault, and the depth at the center of the fault.

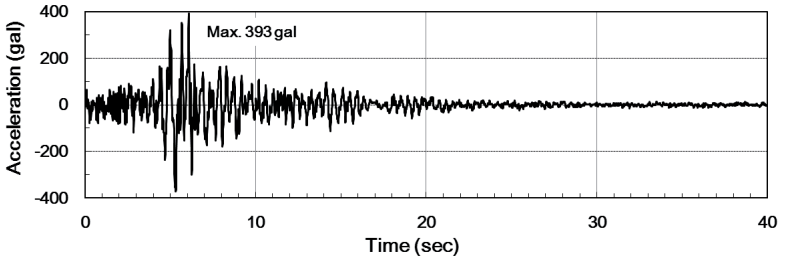

(1) Up and downstream direction

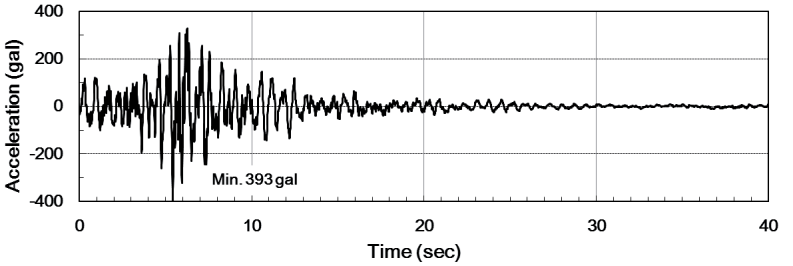

(2) Dam axis direction

Fig. 6
Minogawa Dam waveform time history after amplitude adjustment
Historique de la forme de l’onde après ajustement de l’amplitude du barrage de Minogawa

The acceleration response spectra for the dam location were obtained by using the specific attenuation formula concerning the abstracted MAE candidates as shown in Fig. 5. In all period ranges, the calculation results fell below the lower limit acceleration response spectrum for the MAE candidate (1), (2), (3), and (5).

The results were a little higher than the lower limit acceleration response spectrum in the long period range of T = 1.5 seconds or higher for MAE candidate (4), but this was discarded because it deviated from the natural period of the dam. The lower limit acceleration response spectrum was decided in the “Guidelines for Seismic Performance Evaluation of Dams during Large Earthquakes” and applied to dams throughout Japan considering the possibility that a hidden fault exists at a dam site that could be with magnitude M6.5.

For the above reasons, the lower limit acceleration response spectrum is set as the Level 2 earthquake motion at Chubetsu Dam.

3.2. PREPARING THE WAVEFORM OF THE LEVEL 2 EARTHQUAKE MOTION

From earthquake waveforms observed at several dam sites in the past, the following two observed waveforms were selected as the source waveform considering the dam type, earthquake type, scale of maximum acceleration, duration, and impact on the dam concerned. The acceleration time history was prepared by adjusting the amplitude of source waveforms so as to fit the target acceleration response spectrum.

Fig. 6 shows the upstream-downstream and the dam axis components of the Minogawa Dam waveform after amplitude adjustment.

a) Minogawa Dam: Earthquake waveform observed at an embankment dam during the Southern Hyogo Prefecture Earthquake in 1995 (M7.3).
b) Hitokura Dam: Earthquake waveform observed at a concrete dam during the Southern Hyogo Prefecture Earthquake in 1995 (M7.3).

4. PREPARING THE ANALYSIS MODEL

The analysis modeling set consists of the embankment dam body, concrete dam body, interface, and foundation bedrock, with the straight axis. A three-dimensional FEM model was used and can reproduce the embanking process of embankment dam during construction works.

Fig. 7 shows finite element mesh of the three-dimensional detailed model. The interface consisting of contact clay, intermediate core and main core, was modeled by using the non-linear boundary elements as shown in Fig. 8. The non-linear boundary elements transmit the compressive force but do not transmit the tensile force. The shear modulus is defined as zero when the occurred shear stress exceeded the shear strength.

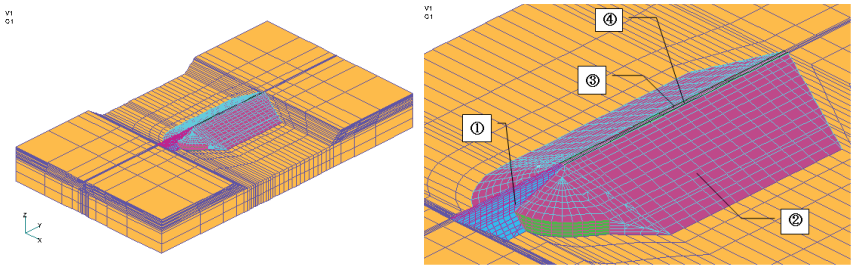

(1) Dam and foundation model (2) Dam body model

Fig. 7
Detailed model element division diagram
Diagramme de division des éléments – Modèle détaillé

1 Concrete dam	*1 Barrage en béton*
2 Shell	*2 Contreforts*
3 Filter	*3 Filtre*
4 Core	*4 Noyau*

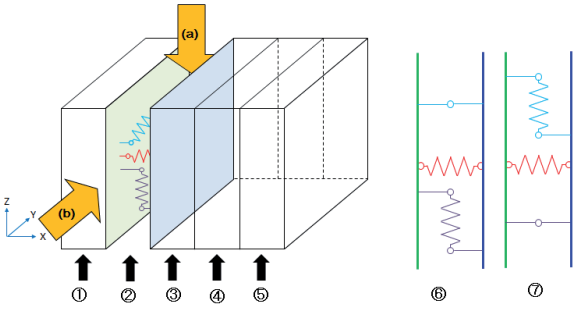

Fig. 8
Non-linear boundary element model of interface
Modèle non linéaire des éléments marginaux limite de l'interface

1 Concrete dam	*1 Barrage en béton*
2 Interface structure	*2 Structure de l'interface*
3 Contact clay	*3 Argile de contact*
4 Core with intermediate grain size	*4 Noyau avec granulométrie intermédiaire*
5 Core	*5 Noyau*
6 Joint element from (b) direction	*6 Elément de jonction dans la direction (b)*
7 Joint element from (a) direction	*7 Elément de jonction dans la direction (a)*

Table 1
Physical properties and shear strength of embankment dam materials

Type of material	Wet density γ_t (kN/m^3)	Saturation density γ_{sub} (kN/m^3)	Coefficient of permeability k (cm/s)	Shear strength	
				Cohesive strength C (kPa)	Angle of internal friction ϕ (°)
Shell	21.5	22.3	1×10^{-1}	88.2	40.7
Filter	22.2	22.6	1×10^{-1}	98.0	40.7
Core	22.1	22.7	1×10^{-5}	5.9	37.2
Intermediate core	20.7	20.7	1×10^{-5}	5.9	37.2
Contact clay	16.2	16.9	1×10^{-5}	9.8	27.1

4.1. PHYSICAL PROPERTIES AND ANALYSIS CONDITIONS

The physical properties of the embankment materials and foundation bedrock were organized and provided as follows.

(1) The wet density, saturated density, and static deformation properties of the embankment dam materials are set based on the quality control testing (average values) during execution. Table 1 shows the physical properties and shear strength of the embankment dam materials.
(2) The dynamic deformation characteristics of the embankment dam materials are set based on the results of a test done during the survey. The dynamic normalized shear modulus G/G0 and the damping ratio h of the material show the strain dependency.
(3) The unit weight, static deformation properties, dynamic deformation properties, and the strength properties of the foundation bedrock are set based on the results of a test done during a survey.
(4) The shear strengths of the shell material and the filter material are provided considering the confining pressure dependency, and the shear strength of the core material is provided based on the quality control testing (average values) during execution based on Mohr-Coulomb's method.
(5) The static properties of the contact clay are set based on laboratory test results. Regarding the static physical properties of the intermediate core, the physical properties adopted are the same as those of the main core, considering the fact that the test grain size of the main core and intermediate core are almost identical.

4.2. COMPARISON OF ANALYSIS AND OBSERVED VALUES

The non-linear properties of the dam body material of the embankment dam part were modeled based on the method of Duncan-Chang et al. [2]. The non-linear static analysis reproducing the banking process was performed to obtain the state of stress caused by the self-weight of the dam body after completion of banking. In order to consider the hydrostatic pressure and seepage force acting on the core zone, seepage analysis for the normal water level was performed. Based on the seepage analysis results, inundation analysis was performed, obtaining the stress distribution of the dam body during inundation. Furthermore, the stress of shell and filter zones on the upstream side below the normal water level were corrected considering the buoyancy.

The calculation results based on the detailed model and the observed values of the horizontal and vertical displacement near the interface surface were compared and obtained good coincidence in vertical component except the bottom area. The calculated displacements are slightly larger than the observed ones in the entire interface surface as shown in Fig. 9.

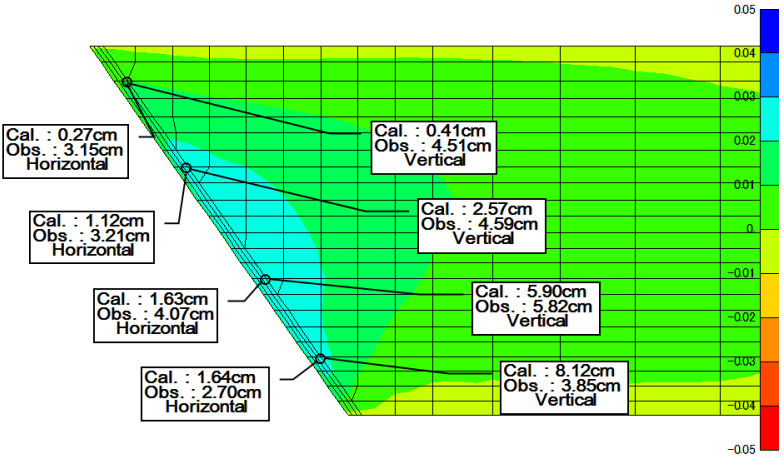

Fig. 9
Comparisons of calculated and observed displacement (4MPa of elastic modulus)
Comparaisons des déplacements calculé et observé (4MPa de module d'élasticité)

5. DYNAMIC ANALYSIS

5.1. DYNAMIC PROPERTIES AND ANALYSIS CONDITIONS

Dynamic analysis using the" equivalent linearizing method "obtains the dynamic stress generated inside the embankment dam body by Level 2 earthquake motion. The state of stress of the dam body during an earthquake was obtained by superimposing the dynamic stress on initial static stress from inundation analysis. The following are the analysis conditions.

(1) The input earthquake motion is given in two directions: the upstream-downstream direction and the dam axis direction. The Level 2 earthquake motion is given at the embankment dam foundation bedrock, so the input earthquake motion to the analysis model is provided at the bottom surface of the model foundation bedrock by using the transmission function to backward calculate the earthquake motion from the bottom surface of the embankment dam foundation bedrock.

(2) The relationships between the shear strain γ, normalized shear modulus G/G_0, and the damping ratio *h* of the embankment dam materials are given as shown in Fig. 10 based on dynamic triaxial test results. Initial shear modulus (G_0) of shell and core are obtained as the function of mean confining pressure σ_m.

(3) The unit weight of the concrete is 23.3 (kN/m^3) and the elastic modulus is 2.5×10^7 (kPa). The elastic modulus of the foundation bedrock is 1.9×10^6 (kPa).

(4) The damping ratio is given as 10% for the concrete dam, as 10% for the embankment dam (added to the material damping ratio), and as 5% for the foundation bedrock.

(5) The water level condition of the reservoir is the normal water level.

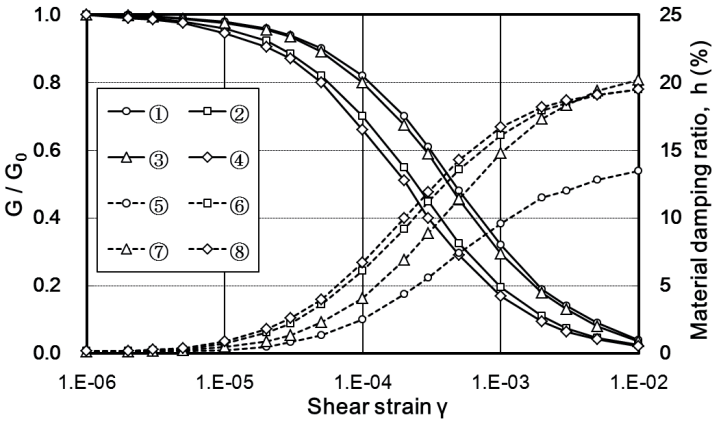

Fig. 10
Relationship of normalized shear modulus (G/G_0) and material damping ratio, h with shear strain γ
Relation entre le module de cisaillement normalisé (G/G0) et le rapport des matériaux d'amortissement, h avec la contrainte de cisaillement γ

1 G/G_0 of shell (G_0 = 1,900 $\sigma_m^{0.64}$)	*1 G/Go des contreforts*
2 G/G_0 of core (G_0 = 1,800 $\sigma_m^{0.67}$)	*2 G/Go du noyau*
3 G/G_0 of upper riverbed gravel	*3 G/G_0 du gravier de lit de rivière supérieur*
4 G/G_0 of lower riverbed gravel	*4 G/Go du gravier du lit de la rivière inférieur*
5 h of shell	*5 h des contreforts*
6 h of core	*6 h du noyau*
7 h of upper riverbed gravel	*7 h du gravier du lit de la rivière supérieur*
8 h of lower riverbed gravel	*8 h du gravier du lit de la rivière inférieur*

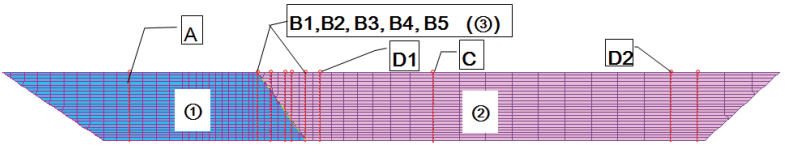

Fig. 11
Location of section where the maximum acceleration was abstracted
Emplacement de la section où l'accélération maximale a été soustraite

1 Concrete dam	*1 Barrage en béton*
2 Embankment dam	*2 Barrage en remblai*
3 Interface structure	*3 Structure de l'interface*

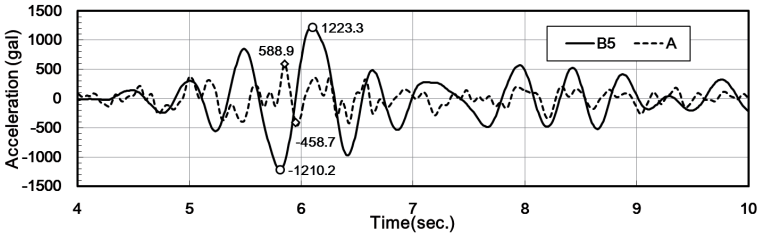

(1) Acceleration time history

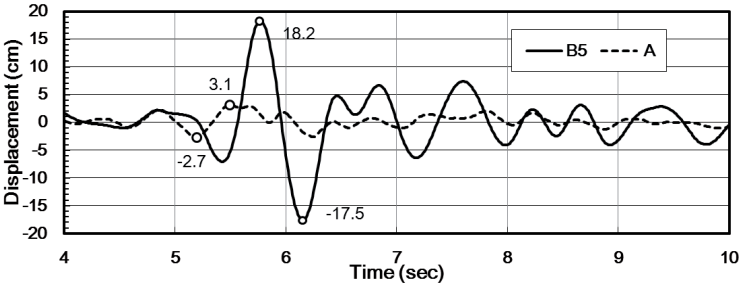

(2) Displacement time history

Fig. 12
Time history of A and B5 at dam crest (upstream–downstream, downstream+)
Historique de A et B5 à la crête du barrage
(en amont-en aval, en aval+)

Next, after dynamic analysis using the equivalent linearizing method, non-linear response analysis is performed in order to evaluate possible separation of the core of the interface and slippage of the interface surface considering the non-linearity of the interface between the embankment dam and the concrete dam. The nonlinear properties of the material in the nonlinear response analysis are artificially considered by using the convergent stiffness from the above-mentioned equivalent linearizing method.

5.2. MAXIMUM ACCELERATION AND MAXIMUM DISPLACEMENT

Fig. 11 shows the locations of the sections where the maximum acceleration and maximum displacement of the dam crest were estimated using the equivalent linearizing method. Section A is the concrete dam part; Section B5 is the largest section of the interface; Section C is near the center of the filter part; and Section D2 is the section near the right bank abutment.

5.2.1. Upstream-Downstream Direction

Table 2
Dynamic analysis results (maximum and minimum acceleration and maximum displacement at dam crest)

Direction of the acceleration	Abstracted section location	Maximum acceleration (cm/s^2)	Minimum acceleration (cm/s^2)	Maximum displacement (cm)
Upstream / downstream direction (Downstream + Upstream -)	A: Concrete dam portion	589	-458	3.1
	B1: Interface	337	-483	4.8
	B2: Interface	512	-642	10.7
	B3: Interface	731	-828	15.0
	B4: Interface	991	-867	16.8
	B5: Interface	1,223	-1,210	18.3
	C: Fill part, center	747	-848	14.6
	D1: Fill part, left bank side	1,008	-1,035	-17.2
	D2: Fill part, right bank side	973	-1,000	16.0
Dam axis direction (Left bank + Right Bank -)	A: Concrete dam portion	308	-334	-3.0
	B1: Interface	255	-259	-3.6
	B2: Interface	280	-421	-5.7
	B3: Interface	415	-577	-7.8
	B4: Interface	495	-663	-9.0
	B5: Interface	632	-839	-11.3
	C: Fill part, center	465	-709	-12.4
	D1: Fill part, left bank side	749	-880	11.4
	D2: Fill part, right bank side	849	-733	-12.6

Fig. 12 shows the acceleration and displacement time histories of Section B5 at the dam crest and Section A at the dam crest. The maximum acceleration at Section B5 at the dam crest where the maximum response was shown in the interface was 1,223 cm/s^2 in the downstream-upstream direction: that is, a response about twice that of Section A in concrete dam part.

The maximum displacement of Section B5 at the dam crest was 18 cm in the upstream and downstream direction: that is, a response about six times that of Section A of the concrete dam part. In the embankment dam part, the maximum acceleration was higher at Section D1 and D2 than Section C of the center of the embankment dam. This is presumed to be a result of the effect of seismic waves transmitted from below the foundation bedrock and of seismic waves input in the diagonal direction from the concrete dam part or the foundation bedrock (see Table 2).

5.2.2. Dam Axis Direction

The maximum acceleration of Section B5 at the dam crest, which shows the maximum response in the interface, was 839 cm/s^2 in the dam axis direction: that is, a response about 2.5 times larger than that of Section A of the concrete dam. The maximum accelerations are larger in Section B5 near the interface, and Section D1 and Section D2 of the embankment dam. The maximum displacement of Section B5 at the dam crest was 11 cm: that is, about four times that of Section A of the concrete dam part (see Table 2).

5.3. TENSILE STRESS OCCURRENCE ON THE INTERFACE AND INTERFACE SURFACE SLIPPAGE

Table 3
Items used to evaluate the seismic resistance of interfaces

Object elements	Occurrence of tensile stress on contact surface	Occurrence of slippage of contact surface	Local safety factor $F_S \geq 1.0$ against shear failure	Continuity of the elements with local safety factor FS < 1.0 against shear failure
Contact clay	○	○	○	○
Intermediate core	-	-	○	○
Main core	-	-	○	○

After dynamic analysis using the equivalent linearizing method, non-linear dynamic analysis was performed considering the non-linearity of the embankment dam and concrete dam interface in order to evaluate the occurrence of tensile stress in the interface core and slippage in the interface surface. The seismic performance evaluation of the interface was performed based on the items shown in Table 3 concerning contact clay, intermediate core, and the main core. The following are the results of the non-linear analysis of Level 2 earthquake motion (Minogawa Dam waveform). Fig. 13 and Fig. 14 show the distribution of the tensile stress and slippage occurrence elements in the interface surface, respectively. It shows the distribution of occurrence elements in the entire time history.

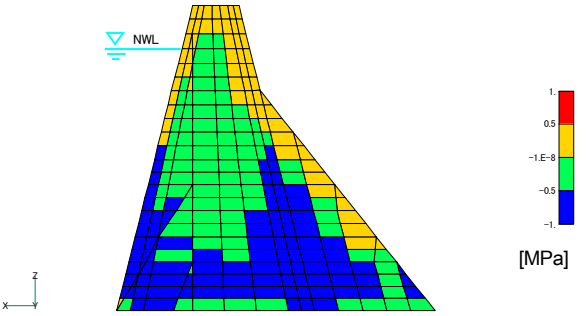

Fig. 13
Distribution of tensile stress occurrence elements inside the interface surface
(+: tensile stress occurrence)
Distribution des éléments occasionnant une contrainte en traction à l'intérieur de la surface de l'interface (+ : apparition de la contrainte de traction)

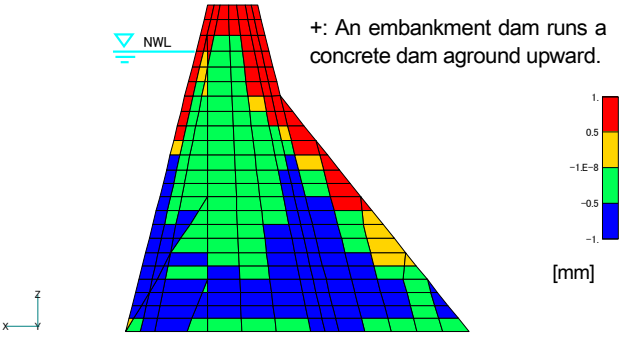

Fig. 14
Distribution of slippage occurrence elements inside the interface surface
Distribution des éléments occasionnant un glissement à l'intérieur de la surface de l'interface

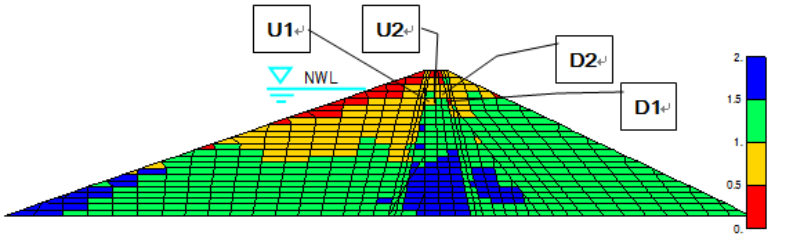

Fig. 15
Distribution of local safety factor against shear (main core, Minogawa Dam waveform, minimum value of time history)
Distribution du facteur de sécurité locale contre le cisaillement (noyau principal, forme de l'onde au niveau du barrage de Minogawa, valeur minimale de l'historique)

(1) The range of occurrence of tensile stress of the contact clay is distributed from the middle elevation to the crest on the upstream end and from the low elevation to the crest on the downstream end. However, near the normal water level, it is not continuous in upstream-downstream direction, so the watertightness of the interface is not harmed.
(2) The range of occurrence of slippage in the interface surface of the contact clay is similarly distributed from the middle elevation to the crest on the upstream end and from the low elevation to the crest on the downstream end. However, near the normal water level, it is not continuous in the upstream-downstream direction, so the watertightness of the interface is not affected.

5.4. LOCAL SAFETY FACTOR AGAINST SHEAR FAILURE OF THE INTERFACE

The local safety factor F_S of element against shear of the contact clay, intermediate core, and core of the interface was obtained for each element based on the stress analysis results from the non-linear analysis. The local safety factor F_S against shear failure was obtained by the following equation (Eq. [1]).

$$F_S = \frac{2C\cos\phi + (\sigma_1 + \sigma_3 - 2u_d)\sin\phi}{(\sigma_1 - \sigma_3)}$$
$$u_d = (1+\nu)(\sigma_{1d} + \sigma_{3d})/3 \qquad [1]$$

Where:

C = cohesion; φ = angle of internal friction; u_d = dynamic pore water pressure; ν = Poisson's ratio; σ_{1d}, σ_{3d} = dynamic maximum principal stress, minimum principal stress.

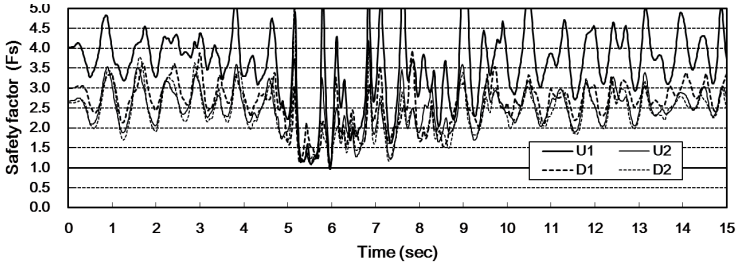

Fig. 16
Time history of local safety factor F_S of object elements (main core, Minogawa Dam waveform)
Historique du facteur de sécurité locale Fs des éléments d'objets (noyau principal, forme de l'onde au niveau du barrage de Minogawa)

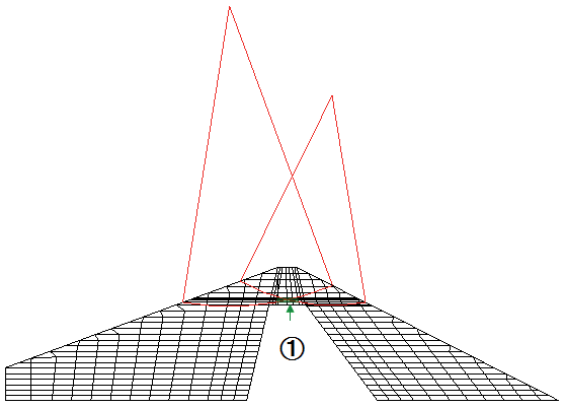

Fig. 17
Sliding stability analysis passing through the core based on the Newmark's method
Analyse de la stabilité au glissement à travers le noyau basée sur la méthode de Newmark

1 Intermediate core *1 Noyau intermédiaire*

Fig. 15 shows the distribution of local safety factor F_S against shear of the main core of the interface, and Fig. 16 shows the time history of the local safety factor of each element near the normal water level. The frequency and cumulative duration of the local safety factors being simultaneously lower than F_S = 1.0 are low and short, respectively.

The local safety factor F_S of the core falls below F_S = 1.0 from near the normal water level on the upstream core side to below normal water level on the downstream side as shown in Fig. 15. An examination of the time history of the local safety factor of each element near the normal water level shows that elements continuous in the upstream-downstream direction simultaneously fall below F_S = 1.0 only one time and for an extremely short duration as shown in Fig. 16. Therefore, the local safety factor momentarily falls below F_S = 1.0 continuously in the upstream-downstream direction. However, it was evaluated that watertightness is not damaged and a sliding plane does not appear to be formed.

For cases in which the elements that fall below the local safety factor F_S = 1.0 in the intermediate core and the main core are continuous in the upstream-downstream direction, the sliding stability analysis were performed based on the Newmark's method by setting hypothetical circular sliding, passing through the intermediate core as shown in Fig. 17 at a section near the normal water level section.

As a result, the minimum safety factor against circular sliding during an earthquake is F_S = 1.59, thus confirming that it exceeds F_S = 1.0. Therefore, it was evaluated that safety against circular sliding during an earthquake from rotational slip of the core is ensured. Here, notice that the minimum safety factor F_S is estimated in the time history of that against circular sliding, and differs from the local safety factor against shear stress calculated for each element shown in Fig. 15.

6. CONCLUSION

Large-scale earthquake motion (Level 2 earthquake motion) was set for near the interface of the embankment dam part and concrete dam part of a large composite dam and the seismic performance mainly near the interface was evaluated. As the Level 2 earthquake motion, the lower limit acceleration response spectrum was set by using the specific attenuation formula for dams to obtain the acceleration response spectrum of the maximum assumption earthquake (MAE) and performing a comparative study. In the part near the interface, the embankment dam and concrete dam, which have different response characteristics, are connected, so a three-dimensional detailed model was prepared and FEM dynamic analysis of the composite dam under Level 2 earthquake motion was carried out to evaluate its seismic performance.

After dynamic analysis using the equivalent linearization method, non-linear dynamic analysis was performed considering the non-linearity of the interface of the embankment dam part and concrete dam part in order to evaluate the possible separation on the interface boundary surface and slippage in the surface. The results show that the range of occurrence of tensile stress in the interface boundary is

distributed at the upstream end and downstream end of the core, but it is not continuous in upstream-downstream direction near the normal water level, so the watertightness of the interface is not harmed. The range of occurrence of slippage in the surface of the interface core is similarly distributed at the upstream end and downstream end of the core, but it is not continuous in the upstream-downstream direction near the normal water level, so the watertightness of the interface is not affected. The local safety factor F_S against shear failure of the main core falls below $F_S = 1.0$ from near the full reservoir water level on the core upstream side to above the normal water level on the downstream side. However, examining the local safety factor F_S of each element near the normal water level shows that the elements continuous in the upstream-downstream direction are simultaneously lower than $F_S = 1.0$ only one time, and the cumulative duration is also extremely short. In the contact clay and the main core of the interface, elements that are momentarily lower than $F_S = 1.0$ are continuous, but it was evaluated that circular sliding is not formed, and watertightness is not affected.

At the interface of a composite dam, contact clay with strong deformation following properties is distributed, and reliable execution work is implemented. Therefore, it was evaluated that the seismic performance against a large-scale earthquake is ensured.

REFERENCES

[1] River Bureau, Ministry of Land, Infrastructure, Transport and Tourism (2005).Guidelines for Seismic Performance Evaluation of Dams against Large Earthquakes (draft). March 2005 (in Japanese).

[2] Duncan, J. M. and Chang, C.Y. (1970). Nonlinear Analysis of Stress and Strain in Soil Mechanics. *Journal of the Soil Mechanics and Foundation Division*. ASCE. SM5. pp.1629~1653. 1970

SUMMARY

This paper sets large-scale earthquake motion (Level 2 earthquake motion) for a large-scale composite dam in order to evaluate seismic performance, mainly near the interface of its embankment dam and concrete dam. In the part near the interface, the embankment dam and concrete dam, which have different response characteristics, are connected, so a detailed three-dimensional model was prepared and three-dimensional FEM dynamic analysis of the composite dam under Level 2 earthquake motion was carried out to evaluate its seismic performance. As the Level 2 earthquake motion, the lower limit acceleration response spectrum (equivalent

to maximum acceleration of 300 cm/s^2) was set by using the specific attenuation formula for dams to obtain the acceleration response spectrum of the maximum assumption earthquake (MAE) and by performing a comparative study.

The results of the dynamic analysis revealed that the range where tension occurred was distributed near the upstream end and downstream end of the interface, but near the normal water level, it was not continuous in the upstream-downstream direction, so the watertightness is not harmed. Similarly, the occurrence of slippage of the interface surface is distributed from the upstream end to the downstream end of the interface, but it is not continuous in the upstream-downstream direction near the normal water level, so its watertightness is not affected. The local safety factor F_S of element against shear failure of the core falls below F_S = 1.0 near the normal water level, but for elements continuous in the upstream-downstream direction, F_S rarely falls below F_S = 1.0, and then for only a very short duration. Therefore, a sliding plane is not formed, and the watertightness is verified.

RÉSUMÉ

Cette étude définit les mouvements d'un tremblement de terre de grande ampleur (mouvements sismiques de niveau 2) dans le cas d'un grand barrage composite afin d'évaluer ses performances sismiques, principalement à proximité de l'interface ou zone de contact du barrage en remblai et du barrage en béton. L'interface relie le barrage en remblai et le barrage en béton, qui présentent des caractéristiques de réponse différentes. Ainsi, un modèle en 3D détaillé a été préparé et une analyse dynamique FEM en 3D du barrage composite dans le cas de mouvements sismiques de niveau a été effectuée en vue d'évaluer les performances en cas de séisme. Au niveau 2 de mouvements sismiques, le spectre de la réponse à l'accélération pour la limite inférieure (l'équivalent d'une accélération maximale de 300 cm/s^2) a été défini en utilisant la formule d'atténuation spécifique pour les barrages afin d'obtenir le spectre de réponse à l'accélération dans le cas d'un séisme supposé d'ampleur maximale (MAE) et au moyen d'une étude comparative.

Les résultats de l'analyse dynamique ont révélé que la plage où la traction apparaît était répartie à proximité des extrémités amont et aval de l'interface, mais qu'à proximité du niveau normal de l'eau, elle n'était pas continue dans le sens amont-aval. Ainsi, l'étanchéité n'était pas affectée. Le facteur local de sécurité F_S des éléments contre une rupture par cisaillement du noyau tombe en-dessous de F_S = 1,0 près du niveau normal de l'eau, mais pour les éléments continus dans le sens amont-aval F_S se situe rarement en dessous de F_S = 1,0 et seulement alors pour une période de temps très courte. Par conséquent, il ne se forme pas de surface plane de glissement, et l'étanchéité a pu être confirmée.